Journal of The Electrochemical Society, **157** (1) E6-E11 (2010)
0013-4651/2009/157(1)/E6/6/$28.00 © The Electrochemical Society

Optimization of AC Electrochemical Etching for Fabricating Tungsten Nanotips with Controlled Tip Profile

S. L. Toh,[z] H. Tan, J. C. Lam, L. C. Hsia,[*] and Z. H. Mai

Chartered Semiconductor Manufacturing Limited, Technology Development Department, Singapore 738406

AC electrochemical etching in diluted potassium hydroxide (KOH) solution was optimized to fabricate tungsten (W) nanotips with a controllable sharpness and aspect ratio using an additional lift-up step. The final tip profile was dependent on the extent of interaction between the KOH solution and the side of the W surface, and effective bubble shielding effects near the apex region during the lift-up. Lateral etching rate along the W material was affected by parameters such as electrolyte–cathode positioning, etching voltage, and electrode size that influenced the flow or replenishment rate of OH^- ions to the W surface submerged in the solution and at the meniscus region. With the lift-up step, the dense layer of bubbles that formed during etching could provide a good shield in minimizing the etch-back effects on the tip apex. Combining the above investigated effects, sharp nanotips with the required aspect ratio could be achieved with the enhanced lateral etching and the protective shield of bubbles.
 [DOI: 10.1149/1.3258289]

Manuscript received August 19, 2009. Published December 2, 2009.

Fabrication of metallic nanotips by electrochemical methodology for nanolithography,[1] scanning probe microscopy,[2-4] and biological cellular studies[5-7] is commonly used because of its simplicity and wide range of selection of etchants. The metal wires can be etched using dc[8,9] or ac,[10] and each etching procedure produces a different tip shape. The hyperboloid shape, as a consequence of the dc "drop-off" method, is well-suited for scanning tunneling microscopy applications.[11] Extensive studies were carried out to investigate the influence of parameters such as applied voltage, cutoff time, depth of wire immersion, height and shape of meniscus, and concentration of electrolyte on preparing tips with a short length, high symmetry, and sharp apex. Recent attempts at dc methodology were also carried out in fabricating long and sharp tips for atomic force microscopy and apertureless near-field scanning optical microscopy by optimizing the conditions for etching long tips,[12] attaching a small Teflon mass to the end of the immersed wire,[13] or using a combination of the drop-off method and dynamic etching.[14] However, its flexibility at the apex regime may make it difficult in applications that require certain degree of robustness, such as nanoindentation[7,15] or nanocharacterization in electronics.[14]

Alternatively, the paraboloidal profile from ac etch has a greater cone angle and is more applicable for enhancing the stiffness near the point of contact with the substrate materials.[7,15] Nonetheless, one major drawback with conventional downward ac electrochemical etching is the difficulty in producing tip apex below 100 nm. During etching, there is a continuous generation of bubbles at the anode that can affect the flow of liquid around the wire.[10] Two effects, the rapid upward stream of bubbles and the perturbed slower convection electrolyte flow, take place simultaneously. Etching rate is not uniform along the immersed wire and is the fastest at the apex where there is little shielding from the surrounding electrolyte. Hence, the majority of the previous studies on ac etching were centered on reducing the apex radius, and the modified etching methods were usually a two-step electrochemical procedure consisting of a normal ac etching and an additional sharpening method. The second step was a fine etching and could be accomplished with reverse upward ac electrochemical etching on pre-etched conical tips[16] or pulsed ac etching with different durations of zero phase.[17] Despite the tremendous efforts made to improve the tip sharpness, the tip apex does not need to be atomically sharp in some applications, and the aspect ratio of the metallic tips near the apex regime may play a more important role instead. For example, multiprobe analysis requires conical-shaped tips of few tenths of nanometer in tip radius, but the cone angle near the apex has to be small for the accommodation of few probes within the nanoscale regime. However, the understanding of the effects of ac etching parameters on the aspect ratio of the tip was not addressed in literature. Methods to counteract the upward stream of bubbles that led to poor aspect ratio and sharpness were also not investigated.

In this paper, we aim to understand the methodology to obtain good control of the resulting tip apex radius and geometry by studying the effects of various etching parameters such as tip movement, electrode position, etching voltage, and electrode size. Specifically, a single-step continuous ac etching was implemented, and the conventional downward etching procedure was modified with an additional lift-up step.

Experimental

Setup.— The electrochemical setup is shown schematically in Fig. 1, and comprises of a cylindrical stainless steel electrode, stainless steel tip holder, variable resistor, multimeter, power supply, and a beaker containing ~0.5 M potassium hydroxide (KOH) solution. Vertical coarse and fine positioning of the wire holder in the *z*-direction was driven by an Oriental motor that was controlled by an external power supply and function generator, and its displacement was observed from a precalibrated counter.

Polycrystalline tungsten (W) wires, with a diameter of ~0.25 mm, were first cut into a length of ~30 mm and cleaned in HF solution to remove its surface oxide. The wire was then mounted upright at the wire holder by screws and was kept close to the center of the cylindrical stainless steel electrode to ensure the uniformity of electric field on all sides of the wire. An initial etching was carried out to remove the presence of any deformed end caused by wire cutting. Around 1 mm of the wire was immersed in the KOH solution and the power supply was switched on. This etching was automatically terminated when the immersed end was completely etched and the power supply was switched off. During the actual etching, 3 mm of the wire was submerged in the KOH solution and an ac power supply of 13.5 V, 50 Hz was applied. The actual potential applied across the etching system was dependent on the variable resistor selected. For each etching parameter such as etching voltage and electrode size, a plot of current vs time was recorded first. The current value at which the tip holder was lifted up was chosen to be the point beyond which there was a sudden drop in the current.

Tip etching.— Figure 2 shows the schematic diagrams of the forces determining the bubble flow in a normal ac electrochemical configuration.[16] For every one half-cycle of the ac voltage, bubbles were formed on the W surface, pressed against the surface, and moved upward along the metal surface in a divergent stream. For the other half-cycle, the W material was electrochemically removed. The resultant etching rate along the surface was determined by two opposing actions: (*i*) the effective contact time between the surrounding electrolyte and metal and (*ii*) the extent of masking effect of the bubbles along the metal surface. In conventional etching illustrated in Fig. 2a, the final tip shape was usually a cone with a

* Electrochemical Society Active Member.
[z] E-mail: tohsl@charteredsemi.com

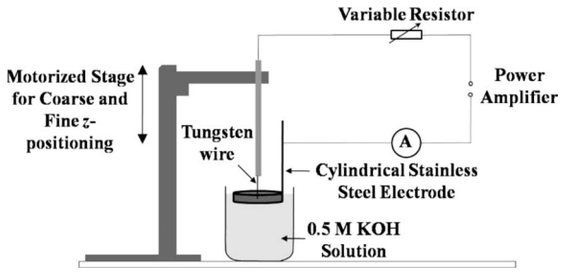

Figure 1. Experimental setup used for the electrochemical setup.

poor sharpness and aspect ratio near the tip apex as a result of differential etching rate along the whole tip profile, with the fastest rate occurring near the bottom of the cone. At each point along the metal surface in Fig. 2a, the buoyant force F_B of the bubbles could be divided into longitudinal component F_L and normal component F_N, which drove the bubbles upward along the surface and pressed the bubbles against the surface, respectively. The bubbles formed a poor shield near the tip apex owing to its density being lower, hence causing weaker shielding at the lower part as compared to the upper portion. The conditions for a better aspect ratio and sharpness could therefore be investigated by having an enhanced lateral reaction between the solution and solid surface with a greater electric field ($E_1 > E_0$), as in Fig. 2b, or having a more effective bubble shielding near the apex in Fig. 2c. In contrast to the conventional downward etching, the setup described in this paper was equipped with a motorized stage to investigate the effects of the bubble dynamics on the etch-back mechanisms of the tip apex. To reap the benefits from the shielding effect of the bubbles, the etched tip was lifted up with the aid of a motorized stage once the selected current value identified from the current–time plot for the submerged etching was reached.

The respective and overall electrochemical reactions at the electrodes can be expressed as follows[9]

Cathode(negative polarity):

$$6H_2O + 6e^- \rightarrow 3H_2(g) + 6OH^- \quad SRP = -2.48 \text{ V}$$

Anode(positive polarity):

$$W(s) + 8OH^- \rightarrow WO_4^{2-} + 4H_2O + 6e^- \quad SOP = +1.05 \text{ V}$$

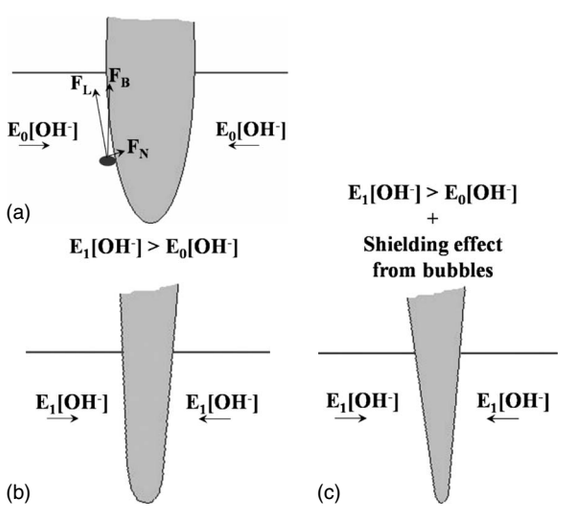

Figure 2. Schematic diagrams of the forces determining the final tip profiles for (a) normal downward ac etching, (b) enhanced lateral etching, and (c) enhanced lateral etching + shielding effect from the bubbles.

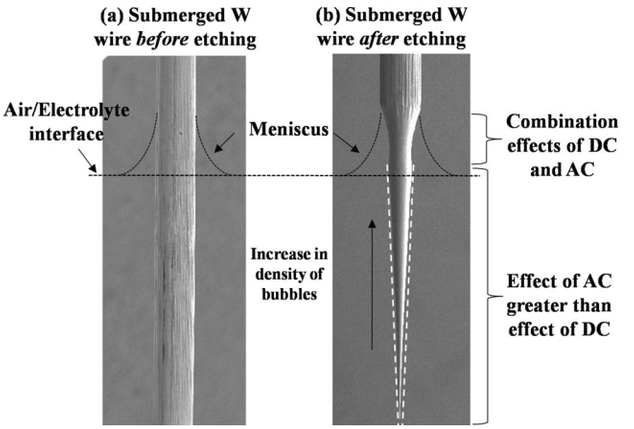

Figure 3. Tip profiles of the submerged W wire (a) before and (b) after ac electrochemical etching.

Overall:

$$W(s) + 2OH^- + 2H_2O \rightarrow WO_4^{2-} + 3H_2(g) \quad E^0 = -1.43 \text{ V}$$

where E^0 is the standard electrode potential given by the sum of the standard reduction potential for water and the standard oxidation potential for W. The above value suggests that the electrochemical reaction can only begin when the applied voltage exceeds 1.43 V. However, for ac in which hydrogen gas has evolved as one of the products, the actual potential required to initiate the reaction is greater.[13] Tip profiles of the submerged W wire (a) before etching and (b) after etching are shown in Fig. 3. Because of the switching electrode behavior from cathode to anode and vice versa for every half-cycle, the final shape of the tip was determined by the interfering effects of OH^- and WO_4^{2-} ions and the density of the bubbles. Near the air/electrolyte interface, the mechanisms were predominantly determined by OH^- and WO_4^{2-} transition zones in which diffusion-limited kinetics and convection-limited kinetics occurred, respectively.[18] The meniscus was formed around the wire at the interface due to the surface tension difference between the air and KOH solution. The concentration of OH^- ions ranged from being the lowest at the top of the meniscus to the highest at the air/electrolyte interface, and the resultant tungstate ions, being denser, flew downward.[9] This had a direct impact on the etching rate at different parts of the W wire within the meniscus region. Underneath the meniscus region in the solution, the density of the bubbles increased with distance away from the tip apex driven by the vertical buoyant force of the bubbles in Fig. 2a. At the intersection point between the highest concentration of tungstate ions and the hydrogen gas, the etching rate was likely to be the slowest within the submerged region as the metal surface was protected from the surrounding OH^- ions. From the scanning electron microscopy (SEM) image in Fig. 3b, this position slightly occurred below the air/electrolyte interface, and the width of the etched W was slightly wider than its vicinity. This region, which could be altered by the flow kinetics of OH^- ions as illustrated in the Results and Discussion section, would have a direct relation to the overall geometry of the tip profile at the tip apex.

Results and Discussion

During normal downward ac electrochemical etching, vigorous hydrogen bubbling periodically occurred at the W wire, leading to a nonuniform etching along the surface of the W wire. Comparing the topography of the tip after (a) normal downward and (b) modified lift-up etching in Fig. 4 under similar etching conditions, there was one region that showed observable difference between the two etching methodology. Shielding effects of the surrounding bubbles during the lift-up step greatly enhanced the aspect ratio near the tip

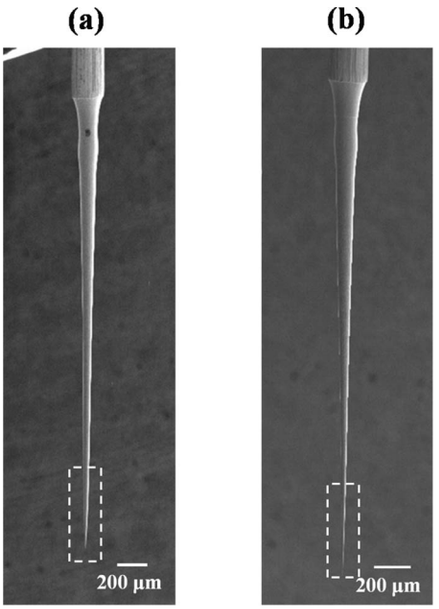

Figure 4. SEM images of the tip profiles obtained for (a) normal downward etching and (b) modified etching. One region that showed obvious difference was observed.

apex, as observed in the lower part of the SEM image taken in Fig. 4b. Nonetheless, the final tip profile obtained was also largely dependent on the following analyzed experimental parameters.

Effects of the lift-up speed.— From the tip apex to the meniscus region, bubble density increased and at the same time, this could counteract the downward stream of the tungstate ions. Under normal downward etching, this caused the lower portion of the tip to be more vulnerable to the attack of the surrounding OH^- ions, therefore inducing greater etching.[10,16] With no shielding, it was difficult to achieve sub-100 nm sharpness for the tip apex. On the contrary, with the protective shield of bubbles after the implementation of the lift-up step, there was a significant improvement in the yield of tips between 50 and 100 nm. Figure 5 shows the dependence of the tip apex radius to the lift-up frequency of the motorized stage in the presence of 0.5 M KOH solution and an effective ac etching voltage of 3.2 V when the determined current value from the current–time plot was reached. Nominal value of ~20 nm sharpness for the radius of curvature (ROC) was achieved when the lift-up speed was 0.10 mm s^{-1}. The schematic diagrams and the SEM images obtained at various lift-up speeds are shown in Fig. 6. To achieve an ROC value of less than 40 nm, a compromise had to be reached in allowing sufficient interaction time between the OH^- ions and the W metal laterally during the lift-up to achieve the desired sharpness. Perturbation of the ascending bubbling flow allowed more OH^- ions to interact alongside of the W surface, leading to enhancement in the lateral etching rate. Nonetheless, when the lift-up frequency of the W tip far exceeded the nominal interaction period illustrated in Fig. 6a, the electrolyte ions would be masked out to a great extent from the tip apex regime, thus retaining its original large tip apex radius effected from the bubble dynamics mechanisms.[9] On the contrary, if the tip holder was drawn up slow, which in this case was less than ~0.05 mm s^{-1}, the effective shielding of the apex region from the surrounding electrolyte was lower, and preferential lateral etching could not be induced at the lower portion of the tip. This therefore resulted in a probe tip with a larger tip apex radius and poor aspect ratio, as shown in Fig. 6b. At low lift-up speed, masking effect from the bubbles at the apex regime was negligible and etching rate on the tip apex was more dependent on the diffusivity of OH^- ions rather than on the lift-up frequency. When the lift-up speed matched close to buoyancy force of the bubbles, as in Fig. 6c, there would still be a certain extent of etching near the tip apex caused by the relatively lower density of bubbles or the perturbed protective downward stream of WO_4^{2-} ions during the lift-up.[15] However, the vertical etching rate was still much lower than that along the side of the W surface, and this was useful in improving the sharpness to ~20 nm, while at the same time enhancing the aspect ratio near the apex regime.

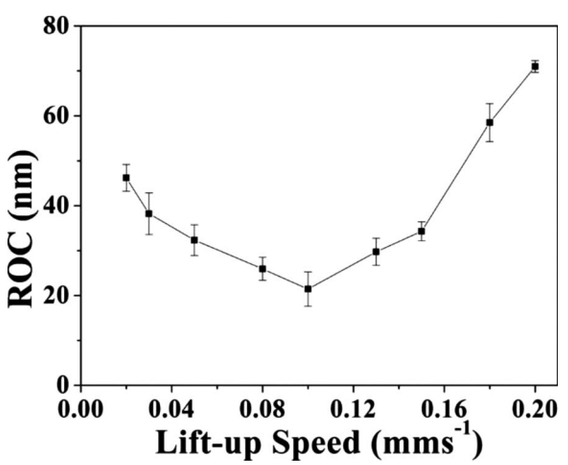

Figure 5. Effects of lift-up speed on the ROC of probe tips.

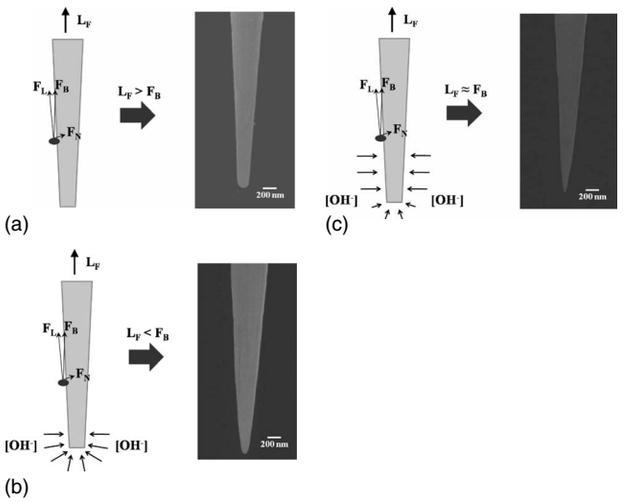

Figure 6. Schematic diagrams of the determining forces during etching and SEM images of the final tip profiles with various lift-up (L_F) speeds, specifically at (a) L_F = 0.20 mm s^{-1}, (b) L_F = 0.02 mm s^{-1}, and (c) L_F = 0.10 mm s^{-1}.

Effects of the electrolyte position relative to the cylindrical stainless steel electrode.— When the wire was immersed in the electrolyte, a meniscus was formed around the W wire due to the surface tension of the aqueous solution. During the electrochemical etching, the rate of diffusion of the OH^- ions to the top of the meniscus was slower than that to the bottom, producing a concave shape at the electrolyte/air interface.[9,19] Nonetheless, the position of the cathode could change the ultimate shape of the meniscus and the aspect ratio of the tip near the tip apex upon the lift-up step. The schematic diagrams that illustrate the relative positions of the cathode [(a) loc1, (b) loc2, (c) loc3, (d) loc4, and (e) loc5] to the level of KOH solution are provided in Fig. 7. SEM images of the tip profiles

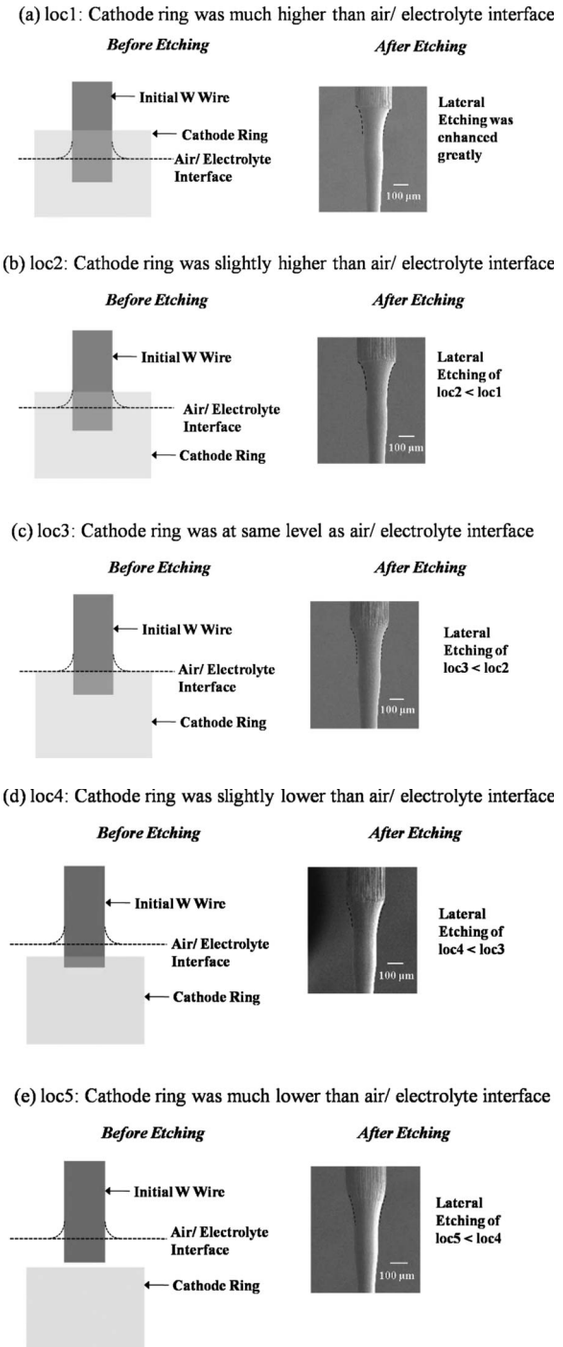

Figure 7. Schematic diagrams and SEM images showing the position of cathode ring to the air/electrolyte interface before etching and the resulting tip profiles after etching, respectively, for (a) loc1, (b) loc2, (c) loc3, (d) loc4, and (e) loc5.

captured at the meniscus region are also shown at different locations. Larger convex meniscus contour was observed in Fig. 7a than in Fig. 7e, for which the cathode ring was placed lower. Taper angles of the tips at about 500 nm away from the tip apex were also calculated and are plotted in Fig. 8. The tips were drawn up at a speed of 0.10 mm s^{-1} when the current value as determined from the current–time plot was reached. The taper angle obtained correlated well to the position of the cathode ring in Fig. 7, in which a progressive increase in the taper angle was observed from loc1 to loc5

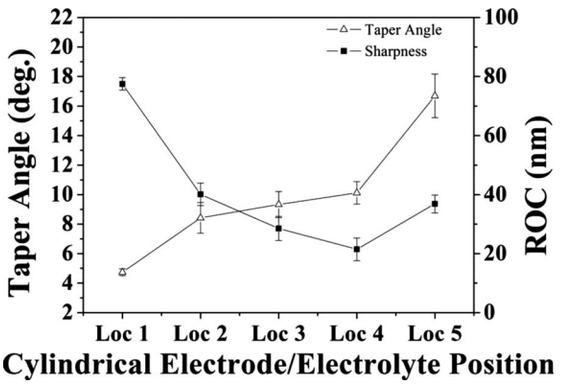

Figure 8. Effects of the KOH level relative to the cathode position on the taper angle and ROC of the probe tips.

where the cathode ring was submerged way below the electrolyte. The behavior at the meniscus regime was predominantly governed by the capillary-gravitational equilibrium, which coincided with a region where the fluid was split into upward and downward flows.[18] The extent of necking phenomenon at the electrolyte/air interface in Fig. 7 was dependent on the removal rates of reaction products along the wire surface.[20] When the upper surface of the cylindrical stainless steel electrode was positioned above the electrolyte, the ion activity of OH^- ions at the electrolyte/air interface was likely to increase laterally. This would still apply during the lift-up step, leading to an enhancement in the aspect ratio, as observed in Fig. 8. When the cylindrical electrode was positioned below the interface, the electric field from the electrode had a smaller impact in directing the OH^- ions horizontally to the upward region of the meniscus, as evidenced from a smaller convex curvature in Fig. 7e. The ultimate interfacial region therefore took the shape of a meniscus that was primarily dictated by the concentration gradient caused by the equilibrium state established by the diffusion of OH^- ions to the W wire and, to a lesser extent, by the bubbling flow for ac electrochemical configuration in Fig. 3. Without the influence of the enhanced electric field during the lift-up, a larger taper angle was observed near the tip apex in Fig. 8 as the extent of lateral etching was reduced. On the contrary, the relative positioning of the cylindrical electrode to the electrolyte had an opposing effect on the tip radii, in which the apex dimensions increased for greater lateral etching as observed at loc1. Nominal conditions were achieved when the electrolyte was around the same level as the cylindrical electrode. At loc5, an etch-back effect could occur owing to less directional flow of OH^- at the interfacial region, resulting in an ultimate increase in the apex radius.

Effects of the etching voltage.— Besides the meniscus effect, the impact of the initial etching voltages, which varied from 1.8 to 5.2 V, was also investigated. As mentioned earlier, when E^0 exceeded 1.43 V, the electrochemical interaction could take place.[9] Nonetheless, the actual value could vary slightly depending on the experimental setup. Figure 9 shows the relationship between the taper angle measured at ~500 nm from the tip apex and the etching voltage applied to the electrochemical etching system. The schematic diagrams that illustrate the postulated etching mechanisms are shown in Fig. 10. The position of the stainless steel cylindrical electrode relative to the air/electrolyte interface was kept the same, and the tips were lifted up with a lift-up speed of 0.10 mm s^{-1} when the determined current value from the current-time plot was reached. With an increase in the voltage, the cone angle decreased as in Fig. 9, indicating an enhancement in the lateral etching upon the lift-up. As illustrated in Fig. 10a, greater electrical voltage, which induced stronger electric field strength between the stainless steel electrode and W wire, was better at directing the flow of OH^- ions toward the W wire, giving rise to larger lateral etching.[21] Lower electric field

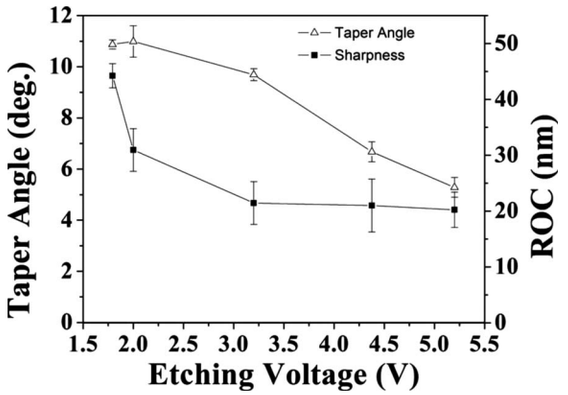

Figure 9. Effects of effective etching voltage on the taper angle and ROC of probe tips.

might result in a more random flow of OH^- ions to the W wire and with no preferential lateral etching along the conical wall. Moreover, penetration of the OH^- ions across the closely packed bubbling stream also became difficult, as described in Fig. 10b. As a result, the etching rate at the lower portion of the W wire was much faster, therefore resulting in tip apex with larger taper angles observed in Fig. 9. Nonetheless, the presence of vigorous bubbling stream at high etching voltages led to a less controllable tip profile, and increased irregularities in the tip profile were observed. When the initial applied voltage was greater than 4.4 V, craters were also observed on the etched surface at times. These were likely to result from microexplosions due to the higher production rates of oxygen and hydrogen at higher applied voltage.[17] This observation was contrary to that observed in dc etching in which smoother etched tips were obtained at higher applied voltage.[12] The optimized tip apex radii for the respective operating voltage are also depicted in Fig. 9. Tip radii progressively decreased from around 1.8 to 3.2 V and after which, an optimized steady apex size of about 20 nm was obtained.

Effects of the size of the cylindrical stainless steel electrode.— The effects on the tip profile governed by the size of the cylindrical electrode were quite similar to that of the etching voltage. Electric field strength is inversely proportional to the distance between the cathode and the anode. Three different sizes of cylindrical stainless steel electrodes normalized to 2.5 cm, which was denoted by D, were investigated. Unlike the effect of etching voltage, modification in the cylindrical electrode dimensions did not demonstrate much distinctive difference in the initial current value, which suggested that the average ion mobilities were not much affected by the size of stainless steel electrode. Figure 11 shows the dependence of the taper angle of the probe tips measured at ~500 nm from the tip apex to the different dimensions of the stainless steel electrode investigated, represented by D, 1.4D, and 2.6D. The etched wires were lifted up with a lift-up speed of 0.10 mm s^{-1} when the current value as determined from the current–time plot was reached. From the graph, the cylindrical electrode with smaller diameter produced tips with smaller taper angle. Figure 12 shows the schematic diagrams that illustrate the flow of ions across the electrochemical setup for the cylindrical stainless steel electrodes with different dimensions, namely, (a) D and (b) 2.6D. In Fig. 12a, a closer proximity between the electrodes was better at directing the diffusion of the ions across the stream of bubbles, giving rise to a larger extent of lateral etching at the side of the wire. The taper angle at the tip apex would be small as long as the etching rate in the lateral direction exceeded that in the vertical direction. For a larger electrode with a diameter of 2.6D in Fig. 12b, permeation of OH^- to the side of the W surface was hindered and the majority of the W/OH^- interactions took place near the tip apex, which had lower density of protective bubbling stream. Preferential etching did not occur laterally and the flow of ions would be more random. The aspect ratio would still be governed to a greater extent by the usual bubble dynamics, resulting in probe tips with greater taper angle. Compared to the overall impact of etching voltage to the size of the cylindrical electrode on the tip profile, etching voltage could more effectively affect the flow of ions to the W surface.

Conclusion

We have successfully demonstrated the capability of downward ac electrochemical etching to fabricate W nanotips with controllable tip profile by incorporating an additional lift-up step implemented by a motorized stage. Poor sharpness and aspect ratio, as a result of the bubble dynamics mechanisms in conventional downward ac etching, could be overcome by enhancing the lateral flow of OH^- to the side of the W surface and using the bubbles as the protective

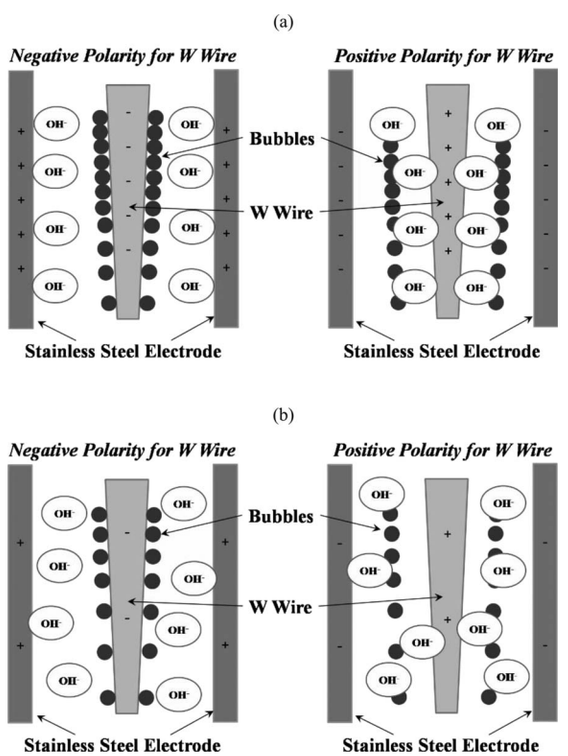

Figure 10. Schematic diagrams illustrating the flow of OH^- ions at (a) high and (b) low etching voltages applied across the electrochemical setup.

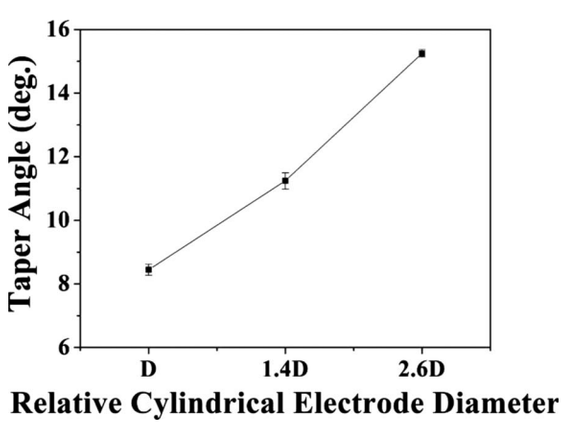

Figure 11. Effects of cathode ring diameter on the taper angle of the probe tips.

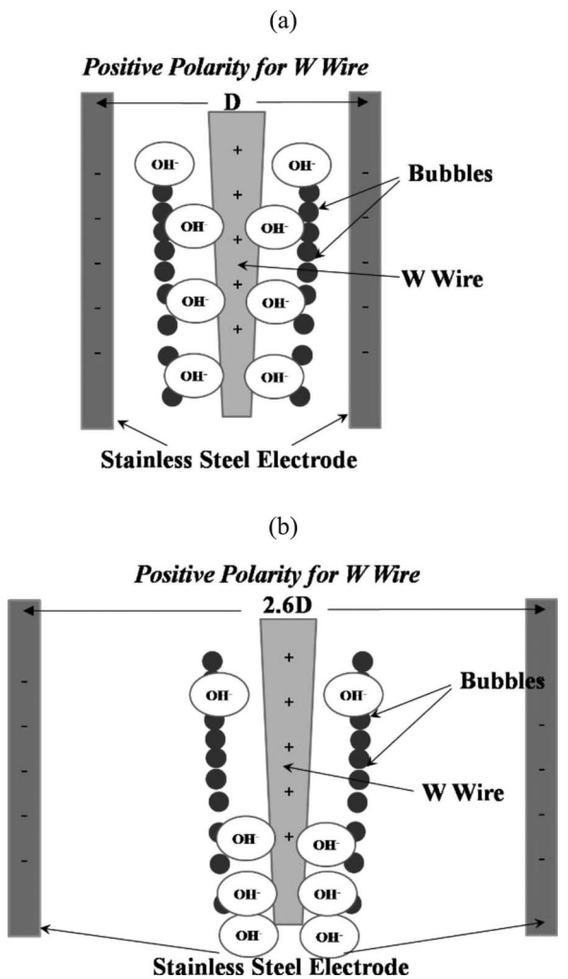

Figure 12. Schematic diagrams illustrating the flow of OH^- ions across the electrochemical setup for cathode ring with diameters of (a) D and (b) 2.6D.

shield to reduce the etch-back effect at the apex region. The optimized etching conditions could be achieved by investigating various etching parameters such as the relative position of the electrolyte and the cylindrical stainless steel electrode, etching voltage, and electrode size. Compared to the extensively used dc methodology, the current study can also be an alternative to obtain nanotips with the required sharpness and aspect ratio for nanoscale applications.

Chartered Semiconductor Manufacturing Ltd. assisted in meeting the publication costs of this article.

References

1. Y. F. Lu, Z. H. Mai, G. Qiu, and W. K. Chim, *Appl. Phys. Lett.*, **75**, 2359 (1999).
2. C. Albonetti, I. Bergenti, M. Cavallini, V. Dediu, M. Massi, J. F. Moulin, and F. Biscarini, *Rev. Sci. Instrum.*, **73**, 4254 (2002).
3. J. P. Song, N. H. Pryds, K. Glejbøl, K. A. Mørch, A. R. Thölén, and L. N. Christensen, *Rev. Sci. Instrum.*, **64**, 900 (1993).
4. M. Cavallini and F. Biscarini, *Rev. Sci. Instrum.*, **71**, 4457 (2000).
5. A. Hermans and R. M. Wightman, *Langmuir*, **22**, 10348 (2006).
6. E. E. El-Giar and D. O. Wipf, *Electroanalysis*, **18**, 2281 (2006).
7. J. F. Graham, K. Griffiths, M. Kovar, P. R. Norton, F. Ogini, and O. L. Warren, *J. Vac. Sci. Technol. A*, **17**, 2240 (1999).
8. A. I. Oliva, G. Romero G., J. L. Peña, E. Anguiano, and M. Aguilar, *Rev. Sci. Instrum.*, **67**, 1917 (1996).
9. J. P. Ibe, P. P. Bey, Jr., S. L. Brandow, R. A. Brizzolara, N. A. Burnham, D. P. DiLella, K. P. Lee, C. R. K. Marrian, and R. J. Colton, *J. Vac. Sci. Technol. A*, **8**, 3570 (1990).
10. M. Fotino, *Rev. Sci. Instrum.*, **64**, 159 (1993).
11. R. Zhang and D. G. Ivey, *J. Vac. Sci. Technol. B*, **14**, 1 (1996).
12. W. X. Sun, Z. X. Shen, F. C. Cheong, G. Y. Yu, K. Y. Lim, and J. Y. Lin, *Rev. Sci. Instrum.*, **73**, 2942 (2002).
13. P. Kim, J. H. Kim, M. S. Jeong, D. K. Ko, J. Lee, and S. Jeong, *Rev. Sci. Instrum.*, **77**, 103706 (2006).
14. R. Hobara, S. Yoshimoto, and S. Hasegawa, *e-J. Surf. Sci. Nanotechnol.*, **5**, 94 (2007).
15. J. C. Grunlan, X. Xia, D. Rowenhorst, and W. W. Gerberich, *Rev. Sci. Instrum.*, **72**, 2804 (2001).
16. M. Fotino, *Appl. Phys. Lett.*, **60**, 2935 (1992).
17. A. H. Sørensen, U. Hvid, M. W. Mortensen, and K. A. Mørch, *Rev. Sci. Instrum.*, **70**, 3059 (1999).
18. M. Kulakov, I. Luzinov, and K. G. Kornev, *Langmuir*, **25**, 4462 (2009).
19. D. W. Xu, K. M. Liechti, and K. Ravi-Chandar, *Rev. Sci. Instrum.*, **78**, 073707 (2007).
20. A. Lazarev, N. Fang, Q. Luo, and X. Zhang, *Rev. Sci. Instrum.*, **74**, 3679 (2003).
21. D. I. Kim and H. S. Ahn, *Rev. Sci. Instrum.*, **73**, 1337 (2002).